INTERNATIONAL JOURNAL FOR NUMERICAL METHODS IN FLUIDS
Int. J. Numer. Meth. Fluids 2003; **43**:1329–1354 (DOI: 10.1002/fld.537)

A staggered conservative scheme for every Froude number in rapidly varied shallow water flows

G. S. Stelling[1,*,†,‡] and S. P. A. Duinmeijer[2,§,¶]

[1] *Fluid Mechanics Section, Faculty of Civil Engineering and Geosciences, Technical University of Delft, P.O. Box 5048, 2600 GA Delft, The Netherlands*
[2] *WL Delft Hydraulics, P.O. Box 177, 2600 MH Delft, The Netherlands*

SUMMARY

This paper proposes a numerical technique that in essence is based upon the classical staggered grids and implicit numerical integration schemes, but that can be applied to problems that include rapidly varied flows as well. Rapidly varied flows occur, for instance, in hydraulic jumps and bores. Inundation of dry land implies sudden flow transitions due to obstacles such as road banks. Near such transitions the grid resolution is often low compared to the gradients of the bathymetry. In combination with the local invalidity of the hydrostatic pressure assumption, conservation properties become crucial. The scheme described here, combines the efficiency of staggered grids with conservation properties so as to ensure accurate results for rapidly varied flows, as well as in expansions as in contractions. In flow expansions, a numerical approximation is applied that is consistent with the momentum principle. In flow contractions, a numerical approximation is applied that is consistent with the Bernoulli equation. Both approximations are consistent with the shallow water equations, so under sufficiently smooth conditions they converge to the same solution. The resulting method is very efficient for the simulation of large-scale inundations. Copyright © 2003 John Wiley & Sons, Ltd.

KEY WORDS: free surface flows; conservation properties; advection; flooding and drying; dam breaks; staggered grids; rapidly varied flow; inundation; bed slope source term

1. INTRODUCTION

Shallow water flow simulations cover a wide range of practical problems, varying from ocean dynamics to flows due to breaking hydro dams. Nowadays there are many numerical methods for the solution of shallow water equations. This paper is devoted to the extension of the applicability of *staggered schemes* to problems that involve rapidly varied flow with a large

*Correspondence to: G. S. Stelling, Fluid Mechanics Section, Faculty of Civil Engineering and Geosciences, Technical University of Delft, P.O. Box 5048, 2600 GA Delft, The Netherlands.
†E-mail: G.S.Stelling@CiTG.TUDelft.nl
‡Professor.
§E-mail: Alex.Duinmeijer@wldelft.nl
¶Project Engineer.

Received 26 May 2002
Revised 20 March 2003

Copyright © 2003 John Wiley & Sons, Ltd.

range of Froude numbers. For examples of *staggered schemes,* see e.g. References [1–3]. These methods are applied mainly to subcritical hydrostatic flows, in one, two and three dimensions, the latter with σ planes, see e.g. Reference [4] or with z planes, see e.g. Reference [5]. Staggered schemes are very often applied for large-scale applications because they have several advantages, such as

- Efficiency in particular in combination with A.D.I. time integration, Leendertse [1], or semi-implicit time integration, e.g. References [2, 6]. The unconditional stability allows deep water, as is often the case in the channels of estuaries, to be simulated next to very shallow water without the time step to be restricted by the deepest part or the smallest grid size.
- Accuracy for subcritical flows due to the fact that the onset of spurious checkerboard modes is avoided without the use of numerical dissipation, e.g. Reference [7].
- Simple and straightforward extension to three-dimensional non-hydrostatic free surface flows, see References [8, 9], or Reference [10], even in combination with unstructured staggered grids, see Reference [11].

Although conservation properties of staggered schemes are well-known topics already since Arakawa [12], yet if methods based upon these principles are applied to rapidly varied flows, such as hydraulic jumps and bores, then the results are often completely incorrect. Use of any non-conservative approach, such as the Eulerian–Lagrangian approach of Casulli [2], also yields incorrect results in these cases. Conservation, as described by Arakawa [12], is mainly applied in long-term integration of large-scale problems, to prevent non-linear instability. This was achieved by global conservation of energy and vorticity. In hydraulic jumps, for instance, energy is dissipated. Thus, energy-conserving methods are not very realistic here, and local conservation of other quantities becomes important. For most of the staggered schemes, flows are supposed to be smooth and sub-critical. (Although an application of a staggered scheme to steady state hydraulic jumps is given for example by Zhou and Stansby [13]). For problems that involve shocks, mainly Riemann solvers or Godunov methods with collocated grids, are successfully applied. They are derived from methods in gas dynamics; see e.g. Reference [14]. Applications of Riemann solvers to shallow water equations are given for example by Glaister [15] and Alcrudo and Garcia Navarro [16]. Flow transitions near steep bed slopes might be a problem for these methods. This problem is related to the so-called *bed slope source terms*, e.g. Reference [17]. In addition, extension of these methods to 3D and to non-hydrostatic flows is not simple at all. These methods often apply explicit time integration. This is not very efficient because large-scale simulations often involve both deep water and shallow water, e.g. estuaries with deep channels and tidal flats. Here time steps restricted by the CFL condition might become very small.

Robust extension of the applicability of staggered schemes to rapidly varied flow is the goal of this paper. It is to be emphasized that, by rapidly varied flow we not only mean shocks with large flow expansions but also strong flow contractions. A key issue of this paper is that in flow contractions, often due to large gradients in the bathymetry, different balance principles apply as in expansions. The problem of bed slope source terms is significantly reduced by numerical approximations that are not only consistent with the shallow water equations but also with elementary physical balance principles in open channel hydraulics, e.g. References [18, 19] (Chapters 3 and 4), where contractions are dealt with in a different way from expansions.

Copyright © 2003 John Wiley & Sons, Ltd.

The resulting method, that is applicable to a wide range of Froude numbers (similar to the so-called Mach uniform method by Bijl and Wesseling [20]), is based upon the following principles:

1. *Mass conservation* combined with non-negative water depths to improve flooding characteristics.
2. *Momentum balance* in flow expansions, to ensure accurate hydraulic jumps and bores.
3. *Energy head conservation* in strong contractions.

We will show that the difference between various balance principles can be viewed as a different interpolation of the advective velocity of momentum from the flow field. Yet we will show that application of a wrong balance principle locally might yield incorrect results. We will show for instance, that application of the momentum principle in a strong contraction could increase the energy head. Due to the guaranteed positive water levels, the application of special *flooding procedures*, as described for instance by Stelling *et al.* [21] or Falconer and Chen [22], can be avoided.

Section 2 of this paper contains a description of the applied numerical techniques for one-dimensional equations. Section 3 describes two-dimensional equations. Section 4 gives results for one-dimensional test problems computed with various balance principles. Section 5 gives a comparison with laboratory experiments.

2. A NUMERICAL METHOD FOR SHALLOW WATER FLOWS WITH LARGE GRADIENTS

2.1. Shallow water equations and sudden transitions

The one-dimensional shallow-water equations in non-conservative form, based on primitive variables, are given by

$$\frac{\partial \zeta}{\partial t} + \frac{\partial (hu)}{\partial x} = 0 \tag{1a}$$

$$\frac{\partial u}{\partial t} + u \frac{\partial u}{\partial x} + g \frac{\partial \zeta}{\partial x} + c_f \frac{u|u|}{h} = 0 \tag{1b}$$

where u is the flow velocity, ζ the water level above plane of reference, c_f the dimensionless bottom friction coefficient, d the depth below reference plane and h the total water depth, $h = \zeta + d$.

At local discontinuities Equations (1) have no unique solution. Some local phenomena, such as almost vertical flow near the upstream slope of a weir, are typically non-hydrostatic. These phenomena are frequently at a scale that is too small to be resolved by a large-scale model; moreover they would require 3D non-hydrostatic free surface flow approximations. However conservation properties, derived from physical considerations, are often sufficient to get solutions that are acceptable in terms of local energy losses, location of a hydraulic jump, propagation speed of a bore, etc. Often conservation of mass and conservation of momentum

Copyright © 2003 John Wiley & Sons, Ltd.

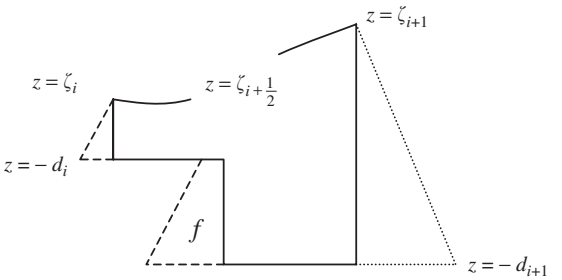

Figure 1. Sudden bed transition.

are applied. For example, for steady flow at a sudden transition, with a constant channel width, as given by Figure 1, a mass balance is applied as follows:

$$q_i = h_i u_i = h_{i+1} u_{i+1} = q_{i+1} \tag{2}$$

where q denotes the depth-integrated velocity.

In a sudden channel expansion the energy head losses are to be derived from application of the momentum principle, (e.g. Reference [19, chapter 4]). For Figure 1 this principle yields a momentum balance that is given by

$$\rho q_i u_i + \tfrac{1}{2}\rho g h_i^2 + f = \rho q_{i+1} u_{i+1} + \tfrac{1}{2}\rho g h_{i+1}^2 \tag{3}$$

where ρ is the constant density of the fluid and f denotes the force per unit width that is exerted by the bed slope onto the fluid. This bed slope force f is given by

$$f = \rho g(\zeta_{i+1/2} + 1/2 d_i + 1/2 d_{i+1})(d_{i+1} - d_i)$$

The difficulty lies in the computation of $\zeta_{i+1/2}$. If we assume that

$$\zeta_{i+1/2} = \gamma\zeta_{i+1} + (1-\gamma)\zeta_i$$

Then, after combination of the hydrostatic forces, Equation (3) can be rewritten as

$$q_{i+1}u_{i+1} - q_i u_i + g((1-\gamma)d_{i+1} + \gamma d_i + \tfrac{1}{2}(\zeta_i + \zeta_{i+1}))(\zeta_{i+1} - \zeta_i) = 0 \tag{4}$$

It follows from Equation (4) that, independent of the value for γ, artificial flow will not be induced because if $\zeta_{i+1} = \zeta_i$ then there is no resulting hydrostatic force.

To get an idea of the head losses, for subcritical flows, Equation (4) combined with Equation (2) is rewritten in dimensionless form as follows:

$$2Fr^2\left(\frac{\alpha+\delta-1}{\alpha+\delta}\right) + (1+\alpha+2\delta(1-\gamma))(1-\alpha) = 0 \tag{5}$$

where

$$Fr = \frac{u_i}{\sqrt{g\zeta_i}}, \quad \alpha = \frac{\zeta_{i+1}}{\zeta_i}, \quad \delta = \frac{d_{i+1}}{\zeta_i}, \quad d_i = 0$$

Copyright © 2003 John Wiley & Sons, Ltd.

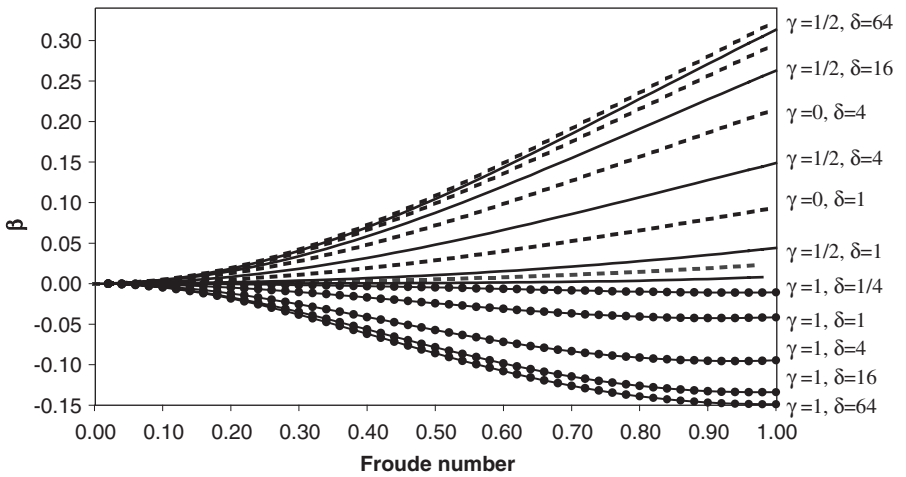

Figure 2. Relative head losses.

The relative head loss β can be defined as

$$\beta = \frac{H_i - H_{i+1}}{H_i} = 1 - \frac{\frac{1}{2}\left(\frac{Fr}{\alpha+\delta}\right)^2 + \alpha}{\frac{1}{2}Fr^2 + 1}$$

where H, the so-called *systematic energy head*, is defined as

$$H = \frac{u^2}{2g} + \zeta$$

Values of β for various given values of γ, δ and Fr $(0 < Fr < 1)$ are given by Figure 2. For $0 \leqslant \gamma \leqslant \pm 0.95$ energy is dissipated whereas for $\gamma = 1$ the energy increases. For low values of Fr the differences between $\gamma = 0$ and $\frac{1}{2}$ are small. For large values of Fr the differences are small in case of large values of δ, i.e. in strong expansions. (Near sudden expansions $\gamma = 0$ is normally assumed.) Equation (5) is symmetric for Fr. This means that if in expansions energy is dissipated, then in contractions there is an increase of energy. Increase of energy is an unrealistic assumption from a physical point of view. In fact in strong contractions the pressure is non-hydrostatic. So any bed slope force in that case, based upon the hydrostatic pressure assumption, is wrong. Therefore, in this situation it is better, perhaps with some additional head losses, to apply the energy head balance[‖]

[‖] In fact in hydraulic engineering it is common practice, in order to estimate reaction forces in contractions, such as the bed slope force, to apply locally, perhaps with some additional head losses, the Bernoulli equation. After this the momentum flux and the hydrostatic forces are computed at locations, upstream and down steam from the contraction, in regions of almost parallel streamlines such that the hydrostatic assumption is valid. The difference between the resulting forces is then assumed to be the reaction force like the bed slope force. This is applied in contractions due to bottom sills, sidewalls or sluice gates.

Copyright © 2003 John Wiley & Sons, Ltd.

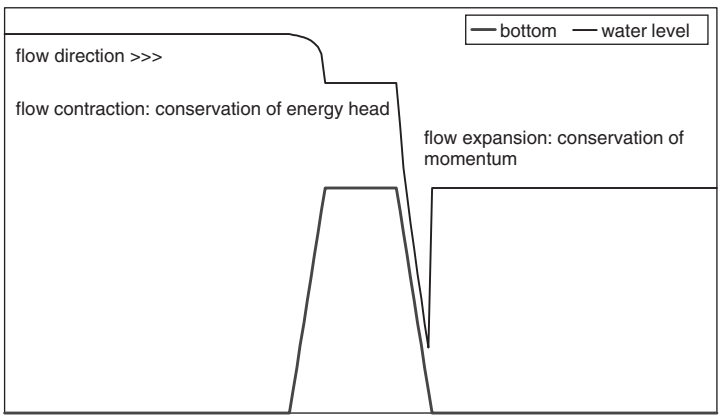

Figure 3. Weir with hydraulic jump.

as given by

$$\frac{u_i^2}{2g} + \zeta_i = \frac{u_{i+1}^2}{2g} + \zeta_{i+1} = \text{constant} \tag{6}$$

Equation (6) is equivalent to the application of the Bernoulli equation (e.g. Reference [19, chapter 3]).

For supercritical flows energy is dissipated in the transition to subcritical flows. Figure 3 shows a broad-crested weir. Here the flow is contracted on the upstream slope of the weir. On the crest the flow is critical. In the transition from the crest to the downstream slope, rather than an expansion, there is further contraction to supercritical flow on the downstream slope. Then, finally, energy is disspated in a hydraulic jump downstream of the weir. Figure 3 shows where to apply conservation of energy head and where to apply conservation of momentum for flow over a weir. Mass conservation has to be applied everywhere.

2.2. *Mass-conservative scheme for water levels*

The bottom does not vary with time. From this it follows that the continuity equation (1a) can be rewritten as

$$\frac{\partial h}{\partial t} + \frac{\partial (hu)}{\partial x} = 0 \tag{7}$$

A common grid for the approximation of Equations (1) is a *staggered grid* as given in Figure 4.

A simple semi-discretization of Equation (7) is given by

$$\frac{\mathrm{d}h_i}{\mathrm{d}t} + \frac{{}^*h_{i+1/2}u_{i+1/2} - {}^*h_{i-1/2}u_{i-1/2}}{\Delta x} = 0 \tag{8}$$

In the staggered grid values denotes as ${}^*h$, are missing at points numbered by $(i + 1/2)$. These points are referred to as *u points*. Here these values are approximated, for example,

Copyright © 2003 John Wiley & Sons, Ltd.

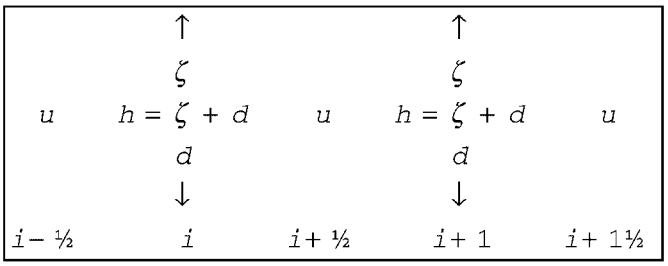

Figure 4. Staggered 1D grid.

by first-order upwinding as follows:

$$ {}^{*}h_{i+1/2} = \begin{cases} h_i, & \text{if } u_{i+1/2} > 0 \\ h_{i+1}, & \text{if } u_{i+1/2} < 0 \\ \max(\zeta_i, \zeta_{i+1}) + \min(d_i, d_{i+1}), & \text{if } u_{i+1/2} = 0 \end{cases} $$

It is obvious that Equation (8) is not only consistent with Equation (1a) but, for steady state conditions, also with Equation (2). More accurate approximations for ${}^{*}h_{i+1/2}$ can be obtained by using slope limiters that are described elsewhere in this paper.

A well-known integration scheme is based upon the θ method. A simple, locally linear, version of this method is given by

$$ \frac{h_i^{n+1} - h_i^n}{\Delta t} + \frac{{}^{*}h_{i+1/2}^n u_{i+1/2}^{n+\theta} - {}^{*}h_{i-1/2}^n u_{i-1/2}^{n+\theta}}{\Delta x} = 0 \tag{9} $$

where $u^{n+\theta} = \theta u^{n+1} + (1-\theta)u^n$.

To derive conditions for non-negative solutions, while we assume positive flow, we rewrite Equation (9) as

$$ h_i^{n+1} = \left(1 - \frac{\Delta t u_{i+1/2}^{n+\theta}}{\Delta x}\right) h_i^n + \frac{\Delta t u_{i-1/2}^{n+\theta}}{\Delta x} h_{i-1}^n $$

with $u_{i+1/2}^{n+\theta} \geqslant 0$, $u_{i-1/2}^{n+\theta} \geqslant 0$.

From this it follows that non-negative water depth is ensured if:

$$ \frac{\Delta t u_{i+1/2}^{n+\theta}}{\Delta x} \leqslant 1 \tag{10} $$

A similar condition can be derived for negative flow. By simply fulfilling inequality (10) water depths will be prevented to become negative, i.e. no special drying and flooding procedures are required for this approach.

It is to be noted that this property of strict non-negative water depths is possible because the equations are formulated with the primitive variable u, instead of the integrated quantity q, $q = uh$.

Copyright © 2003 John Wiley & Sons, Ltd.

2.3. Momentum conservative advection approximations

The so-called momentum conserving formulation of (1b) is given by

$$\frac{\partial}{\partial t}(hu)+\frac{\partial}{\partial x}(hu^2+\tfrac{1}{2}gh^2)+c_{\mathrm{f}}u|u|=gh\frac{\partial d}{\partial x} \tag{11}$$

The right-hand side of this equation is the bed slope source term, normalized with the density. For the description of our numerical method it is convenient to denote the following identities:

$$u\frac{\partial u}{\partial x}=\frac{1}{h}\left(\frac{\partial(hu^2)}{\partial x}-u\frac{\partial(hu)}{\partial x}\right)=\frac{1}{h}\left(\frac{\partial(qu)}{\partial x}-u\frac{\partial q}{\partial x}\right)$$

A spatial discretization for conservation of momentum is given by

$$\frac{\mathrm{d}u_{i+1/2}}{\mathrm{d}t}+\frac{1}{\bar{h}_{i+1/2}}\left(\frac{\bar{q}_{i+1}{}^{*}u_{i+1}-\bar{q}_i{}^{*}u_i}{\Delta x}-u_{i+1/2}\frac{\bar{q}_{i+1}-\bar{q}_i}{\Delta x}\right)+g\frac{\zeta_{i+1}-\zeta_i}{\Delta x}+c_{\mathrm{f}}\frac{|u_{i+1/2}|u_{i+1/2}}{\bar{h}_{i+1/2}}=0 \tag{12}$$

where

$$\bar{h}_{i+1/2}=\frac{h_i+h_{i+1}}{2},\quad \bar{q}_i=\frac{q_{i+1/2}+q_{i-1/2}}{2}\quad\text{and}\quad q_{i+1/2}={}^{*}h_{i+1/2}u_{i+1/2}$$

Similar to the continuity equation, ${}^{*}u_i$ values are now missing at ζ *points*. These missing values are approximated by first-order upwinding as follows:

$${}^{*}u_i=\begin{cases}u_{i-1/2}, & \text{if } \dfrac{q_{i+1/2}+q_{i-1/2}}{2}\geqslant 0\\[2ex] u_{i+1/2}, & \text{if } \dfrac{q_{i+1/2}+q_{i-1/2}}{2}<0\end{cases}$$

Momentum conservation of Equation (12) follows from multiplying this equation by $\bar{h}_{i+1/2}$ and from:

$$\frac{\mathrm{d}\bar{h}_{i+1/2}}{\mathrm{d}t}=-\frac{\bar{q}_{i+1}-\bar{q}_i}{\Delta x},$$

this yields:

$$\frac{\mathrm{d}}{\mathrm{d}t}(\bar{h}_{i+1/2}u_{i+1/2})+\frac{\bar{q}_{i+1}{}^{*}u_{i+1}-\bar{q}_i{}^{*}u_i}{\Delta x}+g\bar{h}_{i+1/2}\frac{\zeta_{i+1}-\zeta_i}{\Delta x}+c_{\mathrm{f}}|u_{i+1/2}|u_{i+1/2}=0$$

Since $\zeta_i=h_i-d_i$, this equation can also be rewritten as

$$\begin{aligned}&\frac{\mathrm{d}}{\mathrm{d}t}(\bar{h}_{i+1/2}u_{i+1/2})+\frac{\bar{q}_{i+1}{}^{*}u_{i+1}-\bar{q}_i{}^{*}u_i}{\Delta x}+\frac{1/2gh_{i+1}^2-1/2gh_{i+1}^2}{\Delta x}+c_{\mathrm{f}}|u_{i+1/2}|u_{i+1/2}\\&\quad=g\bar{h}_{i+1/2}\frac{d_{i+1}-d_i}{\Delta x}\end{aligned} \tag{13}$$

Equation (13) is consistent with Equation (11) and is momentum conservative. Equation (12) is completely equivalent with Equation (13) but does not contain a bed slope source term.

Copyright © 2003 John Wiley & Sons, Ltd.

Hence, given a free surface without any gradient, artificial flow due to this term is impossible. For steady flow with steep bed slopes Equation (13) is consistent with Equation (14) with $\gamma = \frac{1}{2}$. Obviously, other values of γ can be implemented as well in the numerical approximation of Equation (11), but only for $\gamma = \frac{1}{2}$ the combined hydrostatic pressure gradient is approximated with second-order accuracy.

For positive flow direction the advection approximation of Equation (12) yields a simple, first-order accurate, expression given by

$$\frac{1}{\bar{h}_{i+1/2}}\left(\frac{\bar{q}_{i+1}u_{i+1/2}-\bar{q}_i u_{i-1/2}}{\Delta x}-u_{i+1/2}\frac{\bar{q}_{i+1}-\bar{q}_i}{\Delta x}\right)=\frac{\bar{q}_i}{\bar{h}_{i+1/2}}\left(\frac{u_{i+1/2}-u_{i-1/2}}{\Delta x}\right)\approx u\frac{\partial u}{\partial x} \tag{14}$$

It is to be noted that all other terms in Equation (12) are second-order accurate.

2.4. Energy head conserving advection approximation

The so-called energy-head conserving formulation of (1b) is given by

$$\frac{\partial u}{\partial t}+\frac{\partial}{\partial x}\left(\frac{1}{2}u^2+g\zeta\right)+c_{\mathrm{f}}\frac{u|u|}{h}=0 \tag{15}$$

For steady flow and for negligible bottom friction this equation implies the following relation describing the constancy of the *energy head*:

$$H=\frac{u^2}{2g}+\zeta=\text{constant} \tag{16}$$

A simple spatial discretization of Equation (15) is given by

$$\frac{\mathrm{d}u_{i+1/2}}{\mathrm{d}t}+\frac{1/2\,{}^{*}u_{i+1}^2-1/2\,{}^{*}u_i^2}{\Delta x}+g\frac{\zeta_{i+1}-\zeta_i}{\Delta x}+c_{\mathrm{f}}\frac{|u_{i+1/2}|u_{i+1/2}}{1/2(h_{i+1}+h_i)}=0 \tag{17}$$

From this it follows that near sudden transitions, where time derivatives and bottom shear stress can be neglected, the following relation holds:

$$\frac{{}^{*}u_i^2}{2g}+\zeta_i=\frac{{}^{*}u_{i+1}^2}{2g}+\zeta_{i+1}$$

which is consistent with Equations (6) and (16).

Again, ${}^{*}u_i$ values are missing at ζ *points*. Again they can be approximated by first-order upwinding as follows:

$${}^{*}u_i=\begin{cases}u_{i-1/2}, & \text{if } \dfrac{u_{i+1/2}+u_{i-1/2}}{2}\geqslant 0\\[2ex] u_{i+1/2}, & \text{if } \dfrac{u_{i+1/2}+u_{i-1/2}}{2}<0\end{cases}$$

For positive values of $u\forall i$, first-order upwinding of u values at ζ *points* yields a first-order advection approximation that is given by

$$\frac{1/2\,{}^{*}u_{i+1}^2-1/2\,{}^{*}u_i^2}{\Delta x}=\frac{1/2u_{i+1/2}^2-1/2u_{i-1/2}^2}{\Delta x}=1/2(u_{i+1/2}+u_{i-1/2})\left(\frac{u_{i+1/2}-u_{i-1/2}}{\Delta x}\right)\approx u\frac{\partial u}{\partial x} \tag{18}$$

Copyright © 2003 John Wiley & Sons, Ltd.

It is to be noted that non-conservative formulations, such as the Eulerian Lagrangian methods, as applied by Casulli [2], when applied with first-order accuracy, yield the following expression:

$$u\frac{\partial u}{\partial x} \approx u_{i+1/2}\left(\frac{u_{i+1/2}-u_{i-1/2}}{\Delta x}\right) \tag{19}$$

On summarizing, every first-order approximation can be denoted as

$$\left(u\frac{\partial u}{\partial x}\right)_{i+1/2} \approx \max(u_{\rightarrow},0)\left(\frac{u_{i+1/2}-u_{i-1/2}}{\Delta x}\right)+\min(u_{\leftarrow},0)\left(\frac{u_{i+l1/2}-u_{i+1/2}}{\Delta x}\right)$$

where the advective velocities $u_{\rightarrow}$ and $u_{\leftarrow}$ depend on the conservation principle as follows: Conservation of momentum:

$$u_{\rightarrow}=\frac{\bar{q}_i}{\bar{h}_{i+1/2}}, \quad u_{\leftarrow}=\frac{\bar{q}_{i+1}}{\bar{h}_{i+1/2}}$$

Conservation of energy head:

$$u_{\rightarrow}=1/2(u_{i+1/2}+u_{i-1/2}), \quad u_{\leftarrow}=1/2(u_{i+1/2}+u_{i+l1/2})$$

No conservation:

$$u_{\rightarrow}=u_{\leftarrow}=u_{i+1/2}$$

From this it follows that the difference between momentum conservation, energy head conservation or no conservation at all, lies in the way in which the advective speed of momentum is interpolated from the flow field.

2.5. *A dynamical conservative scheme*

In principle the choice between Equations (14) and (18) can be based upon a simple dynamic algorithm as follows:

If $\dfrac{u_{i+1/2}-u_{i-1/2}}{\Delta x}>\varepsilon>0$ then use Equation (18) else use Equation (14).

By the choice of ε it is possible to apply energy head conservation only in strong flow contractions, such that elsewhere momentum conservation is applied.

2.6. *Improved numerical accuracy*

The proposed method so far is only of first-order accuracy. 'Almost second-order approximations', including guaranteed non-negative water depth, can be constructed as well. For this purpose the missing u values at ζ points and vice versa are approximated by upwinded second-order extrapolation in combination with *slope limiters*, similar to the *flux limiters* as described by Hirsch [23]. The slope limited approximations guarantee that the water levels are not negative for sufficiently small time steps. The local order of consistency depends on the solution. Near extreme values the accuracy reduces to first-order elsewhere the approximation is second-order accurate.

Copyright © 2003 John Wiley & Sons, Ltd.

For positive flow direction the extrapolations are given by

$$^{*}u_i = u_{i-1/2} + \tfrac{1}{2}\Psi(r_u)(u_{i-1/2} - u_{i-3/2}) \tag{20}$$

$$^{*}h_{i+1/2} = h_i + \tfrac{1}{2}\Psi(r_\zeta)(\zeta_i - \zeta_{i-1}) \tag{21}$$

Here $\Psi(r)$ denotes the slope limiter. For $h_{i+1/2}$ the limiter is only applied to the water level. The total number of possible slope limiters is large. As an example we give the *minmod limiter* and the *Van Leer limiter* that are given by

$$\text{Minmod: } \Psi(r) = \max(0, \min(r, 1)), \quad \text{Van Leer: } \Psi(r) = \frac{r + |r|}{1 + r}$$

where r is given by: $r_u = \dfrac{u_{i+1/2} - u_{i-1/2}}{u_{i-1/2} - u_{i-3/2}}$ or $r_\zeta = \dfrac{\zeta_{i+1} - \zeta_i}{\zeta_i - \zeta_{i-1}}$

For negative flow direction, the limiters are defined accordingly.

Although monotonicity is not a characteristic of the solution of the equations as such, yet the limiters are useful to improve the accuracy of the model results without the generation wiggles.

3. TWO-DIMENSIONAL APPROXIMATIONS

The 1D method described here can easily be extended to two dimensions. For this purpose we consider the 2D shallow water equations as given by

$$\frac{\partial \zeta}{\partial t} + \frac{\partial (uh)}{\partial x} + \frac{\partial (vh)}{\partial y} = 0 \tag{22a}$$

$$\frac{\partial u}{\partial t} + u\frac{\partial u}{\partial x} + v\frac{\partial u}{\partial x} + g\frac{\partial \zeta}{\partial x} + c_{\mathrm{f}}\frac{u\|u\|}{h} = 0 \tag{22b}$$

$$\frac{\partial v}{\partial t} + u\frac{\partial v}{\partial x} + v\frac{\partial v}{\partial y} + g\frac{\partial \zeta}{\partial y} + c_{\mathrm{f}}\frac{v\|u\|}{h} = 0 \tag{22c}$$

where u and v are now the x and y components of the depth averaged velocity vector.

Figure 5 defines a staggered numerical grid. A mass conservative approximation of Equation (22a) is given by

$$\frac{\mathrm{d}\zeta_{i,j}}{\mathrm{d}t} + \frac{^{*}h_{i+1/2,j}u_{i+1/2,j} - {}^{*}h_{i-1/2,j}u_{i-1/2,j}}{\Delta x} + \frac{^{*}h_{i,j+1/2}v_{i,j+1/2} - {}^{*}h_{i,j-1/2}v_{i,j-1/2}}{\Delta y} = 0 \tag{23}$$

A momentum conservative spatial discretization of Equation (22b), (22c), while assuming positive flow directions, can now be given by

$$\frac{\mathrm{d}u_{i+1/2,j}}{\mathrm{d}t} + \frac{\overline{{}_{u}q}^{x}_{i,j}}{\bar{h}^{x}_{i+1/2,j}}\frac{u_{i+1/2,j} - u_{i-1/2,j}}{\Delta x} + \frac{\overline{{}_{v}q}^{x}_{i,j-1/2}}{\bar{h}^{x}_{i+1/2,j}}\frac{u_{i+1/2,j} - u_{i+1/2,j-1}}{\Delta y}$$
$$+ g\frac{\zeta_{i+1,j} - \zeta_{i,j}}{\Delta x} + c_{\mathrm{f}}\frac{u_{i+1/2,j}\|u_{i+1/2,j}\|}{\bar{h}^{x}_{i+1/2,j}} = 0 \tag{24}$$

Copyright © 2003 John Wiley & Sons, Ltd.

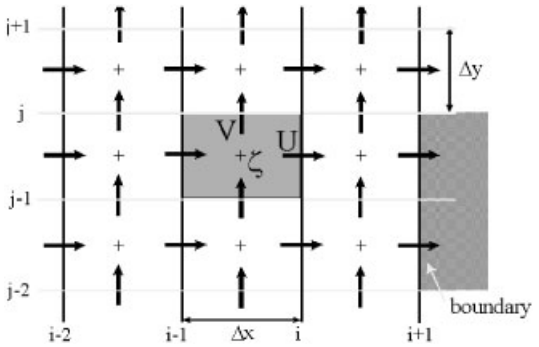

Figure 5. Staggered 2D grid.

$$\frac{\mathrm{d}v_{i,j+1/2}}{\mathrm{d}t} + \frac{\overline{{}_uq}^{y}_{i-1/2,j}}{\bar{h}^{y}_{i,j+1/2}} \frac{v_{i,j+1/2} - v_{i-1,j+1/2}}{\Delta x} + \frac{\overline{{}_vq}^{y}_{i,j}}{\bar{h}^{y}_{i,j+1/2}} \frac{v_{i,j+1/2} - v_{i,j-1/2}}{\Delta y} + g\frac{\zeta_{i,j+1} - \zeta_{i,j}}{\Delta y} + c_{\mathrm{f}} \frac{v_{i,j+1/2}\|u_{i,j+1/2}\|}{\bar{h}^{y}_{i,j+1/2}} = 0 \tag{25}$$

where: ${}_uq = uh$, ${}_vq = vh$, $\bar{h}^{x}_{i+1/2,j} = (h_{i,j} + h_{i+1,j})/2$, $\bar{h}^{y}_{i,j+1/2} = (h_{i,j} + h_{i,j+1})/2$ and all other values are defined accordingly. For negative flow directions the formulation is similar.

The momentum conservation characteristics follow from multiplying Equations (24) and (25) by $\bar{h}^{x}$ and $\bar{h}^{y}$, respectively and adding, to each of the equations, Equation (23), in averaged form over two grid points, and multiplied by u or v.

Energy conserving approximations are given by

$$\frac{\mathrm{d}u_{i+1/2,j}}{\mathrm{d}t} + \bar{u}^{x}_{i,j} \frac{u_{i+1/2,j} - u_{i-1/2,j}}{\Delta x} + \bar{v}^{x}_{i,j-1/2} \frac{u_{i+1/2,j} - u_{i+1/2,j-1}}{\Delta y} + g\frac{\zeta_{i+1,j} - \zeta_{i,j}}{\Delta x} + c_{\mathrm{f}} \frac{u_{i+1/2,j}\|\bar{\bar{u}}_{i+1/2,j}\|}{\bar{h}^{x}_{i+1/2,j}} = 0 \tag{26}$$

$$\frac{\mathrm{d}v_{i,j+1/2}}{\mathrm{d}t} + \bar{u}^{y}_{i-1/2,j} \frac{v_{i,j+1/2} - v_{i-1,j+1/2}}{\Delta x} + \bar{v}^{y}_{i,j} \frac{v_{i,j+1/2} - v_{i,j-1/2}}{\Delta y} + g\frac{\zeta_{i,j+1} - \zeta_{i,j}}{\Delta y} + c_{\mathrm{f}} \frac{v_{i,j+1/2}\|\bar{\bar{u}}_{i,j+1/2}\|}{\bar{h}^{y}_{i,j+1/2}} = 0 \tag{27}$$

The double overbar denotes that the velocity norm is computed by means of averaging.

It is to be noted that conservation of energy head is a principle that is applied along a stream line. Since the grid, unlike the 1D case, does not coincide with the stream lines, Equations (26) and (27) are not precisely equivalent to the Bernoulli equation along a stream line. However, they will not generate energy locally and the local dissipation of energy will be small.

Copyright © 2003 John Wiley & Sons, Ltd.

Time integration can be implemented with semi-implicit methods according to References [2, 6] or with ADI according to Reference [24]. Time integration is based upon the θ method. For $\theta = 0.5$ this method is precisely momentum conservative, but non-linear. A linearized version is given by

$$\frac{\zeta_{i,j}^{n+1} - \zeta_{i,j}^{n}}{\Delta t} + \frac{{}^{*}h_{i+1/2,j}^{n} u_{i+1/2,j}^{n+\theta} - {}^{*}h_{i+1/2,j}^{n} u_{i+1/2,j}^{n+\theta}}{\Delta x} + \frac{{}^{*}h_{i,j+1/2}^{n} v_{i,j+1/2}^{n+\theta} - {}^{*}h_{i,j-1/2}^{n} v_{i,j-1/2}^{n+\theta}}{\Delta y} = 0 \tag{28a}$$

$$\frac{u_{i+1/2,j}^{n+1} - u_{i+1/2,j}^{n}}{\Delta t} + u_{\rightarrow}^{n} \frac{u_{i+1/2,j}^{n} - u_{i-1/2,j}^{n}}{\Delta x} + v_{\uparrow}^{n} \frac{u_{i+1/2,j}^{n} - u_{i+1/2,j-1}^{n}}{\Delta y} + g \frac{\zeta_{i+1,j}^{n+\theta} - \zeta_{i,j}^{n+\theta}}{\Delta x} + c_{\mathrm{f}} \frac{u_{i+1/2,j}^{n+1} \|\bar{\bar{u}}_{i+1/2,j}^{n}\|}{(\bar{h}^{x})_{i+1/2,j}^{n}} = 0 \tag{28b}$$

$$\frac{v_{i,j+1/2}^{n+1} - v_{i,j+1/2}^{n}}{\Delta t} + u_{\rightarrow}^{n} \frac{v_{i,j+1/2}^{n} - v_{i-1,j+1/2}^{n}}{\Delta x} + v_{\uparrow}^{n} \frac{v_{i,j+1/2}^{n} - v_{i,j-1/2}^{n}}{\Delta y} + g \frac{\zeta_{i,j+1}^{n+\theta} - \zeta_{i,j}^{n+\theta}}{\Delta x} + c_{\mathrm{f}} \frac{v_{i,j+1/2}^{n+1} \|\bar{\bar{u}}_{i,j+1/2}^{n}\|}{(\bar{h}^{y})_{i,j+1/2}^{n}} = 0 \tag{28c}$$

For flooding over a dry bed a predictor corrector approach is applied for bottom friction. This prevents overshoot of the velocities if the velocity accelerates from zero during the passage of a flow discontinuity.

The linear equations resulting from the Equations (28) are symmetric and positive definite; hence a CG method can be applied to solve the equations efficiently, similar to Casulli and Catani [2]. The condition (5) is now also a stability condition, see also Reference [2]. Unconditional stability can be obtained by using an integration scheme as described by [24].

4. NUMERICAL EXAMPLES OF 1D FLOWS WITH LARGE GRADIENTS

This section describes three frictionless 1D test problems. The first example is related to subcritical flows, it demonstrates the differences between different methods for the advection approximation in cases of sudden contractions or sudden expansions, without shocks. The other examples are related to hydraulic jumps and bores. The examples, of which analytical solutions can be constructed, are used by many authors e.g. Reference [25].

4.1. Subcritical sudden contractions and expansions

For this example, consider a frictionless channel with a constant width and a length of 100 m. Upstream a depth-integrated velocity is given of 1 m^2/s. At the down stream end a water level is prescribed of 1 m. The bottom profile is such that: (case I) sudden expansions are

Copyright © 2003 John Wiley & Sons, Ltd.

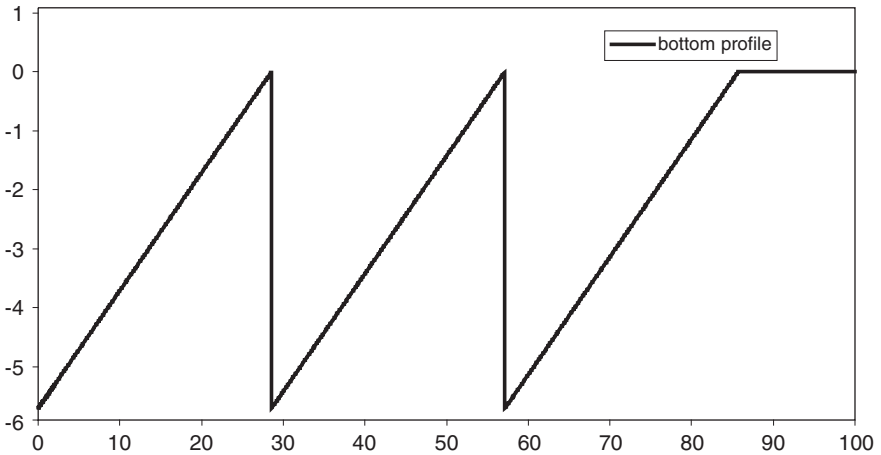

Figure 6. Bed profile with sudden expansions.

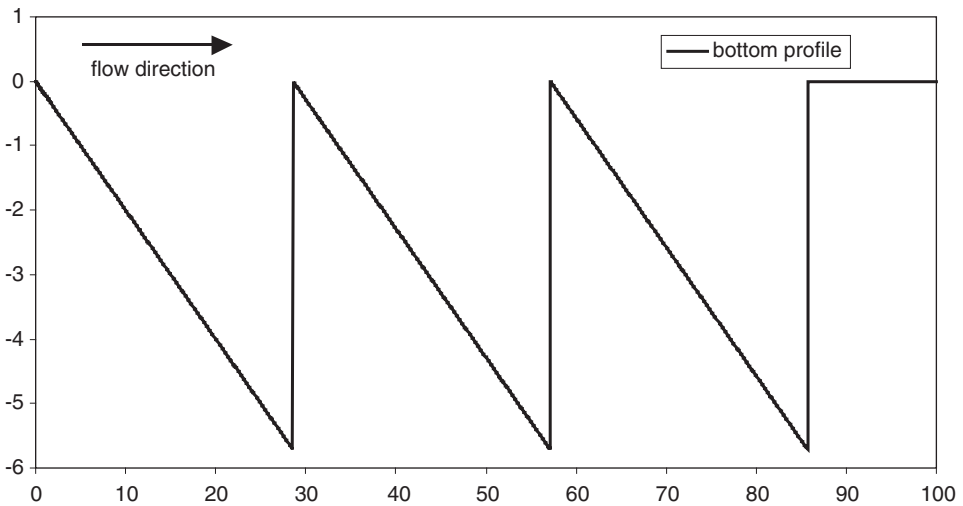

Figure 7. Bed profile with sudden contractions in the flow direction.

followed by gradual contractions and (case II) sudden contractions are followed by gradual expansions. The bottom profiles are given by Figures 6 and 7. The maximum Froude number for this test is 0.32, so the flow is subcritical everywhere. Based on physical considerations it is to be expected that head losses will only take place near the sudden expansions. To verify this with numerical computations we consider the following approximations of the advective term in the momentum equation:

$$u\frac{\partial u}{\partial x} \approx 1/2(u_{i+1/2} + u_{i-1/2})\left(\frac{u_{i+1/2} - u_{i-1/2}}{\Delta x}\right) \tag{18}$$

Copyright © 2003 John Wiley & Sons, Ltd.

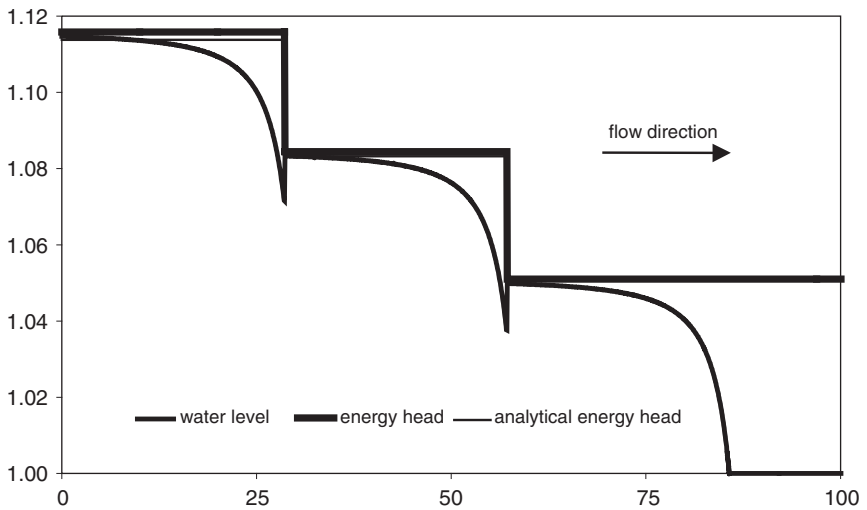

Figure 8. Water levels and energy line with methods B, C and D for sudden bed expansions.

$$u\frac{\partial u}{\partial x} \approx \frac{\bar{q}_i}{\bar{h}_{i+1/2}}\left(\frac{u_{i+1/2}-u_{i-1/2}}{\Delta x}\right) \tag{14}$$

$$u\frac{\partial u}{\partial x} \approx u_{i+1/2}\left(\frac{u_{i+1/2}-u_{i-1/2}}{\Delta x}\right) \tag{19}$$

Application of the energy head conserving Equation (18) only, will be defined as *Method A*, application of the momentum conserving Equation (14) only, will be defined as *Method B*, application of Equation (18) in contractions and of Equation (14) in expansions will be defined as *Method C* and finally application of the non-conservative Equation (19) only, will be defined as *Method D*. This method is similar to the Eulerian Lagrangian method that is applied by Casulli [2].

For case I the results the Method B, C and D, are given by Figure 8. Each of these methods yields the same energy head loss at the sudden expansions. The differences with the analytical solution are small. Method A is energy head conservative and shows no head losses, not even at the expansions, as is shown by Figure 9.

For case II, with bed profile as given by Figure 7, the results of Method B are given in Figure 10. At each sudden contraction the energy head is increased, this yields a total increase of the water level of 0.1 over 100 m. It confirms our remark earlier that the momentum principle is symmetric in the sense that when head losses occur near expansions then, like wise, head gains are obtained near contractions. This result is totally wrong from a physical point of view. It demonstrates clearly that the momentum principle should be applied with care and not as a rigorous approach to solve shallow water equations also in regions with sudden contractions. Numerical stability problems are a possible side effect of increasing the energy head. In this respect it is to be realised that flow contractions are also induced by contractions of the channel width.

Copyright © 2003 John Wiley & Sons, Ltd.

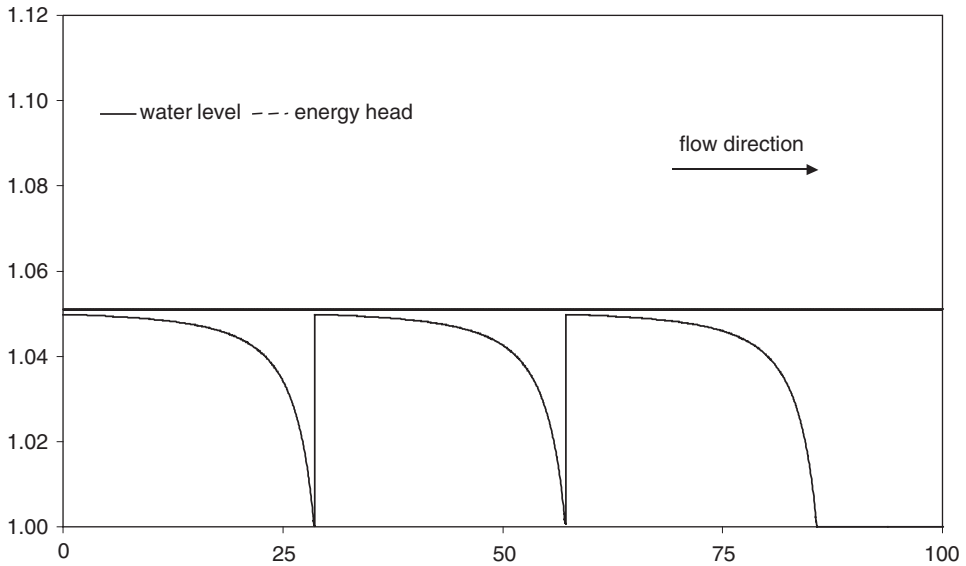

Figure 9. Water levels and energy line for energy head conservative approximation.

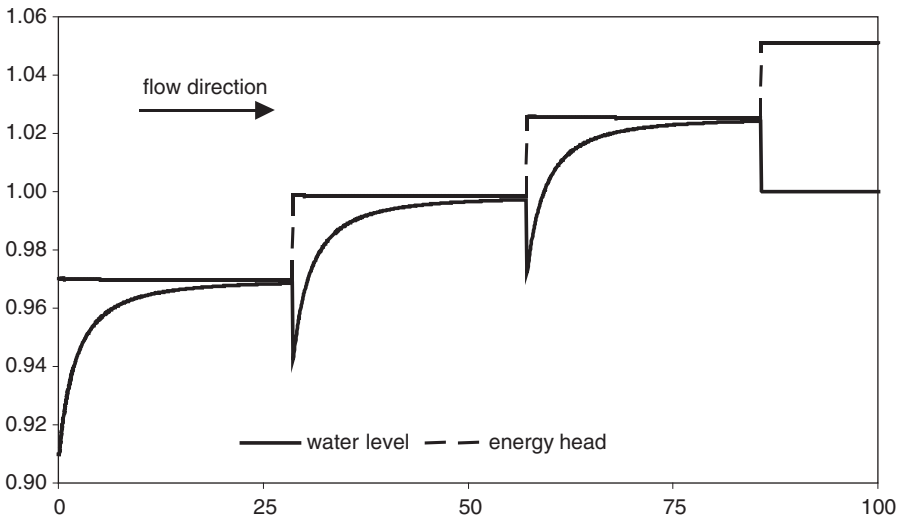

Figure 10. In flow direction increasing water levels and energy line for momentum conservative approximations.

Method C yields the results given by Figure 11. There are hardly head losses in this case, so the results are very similar to Method A that is therefore not plotted. The results of Method D are given in Figure 12. This non-conservative approach reveals dissipation at every sudden transition. It does not seem to make much difference whether the sudden transition is a contraction or an expansion. From a stability point this is therefore the most robust approach.

Copyright © 2003 John Wiley & Sons, Ltd.

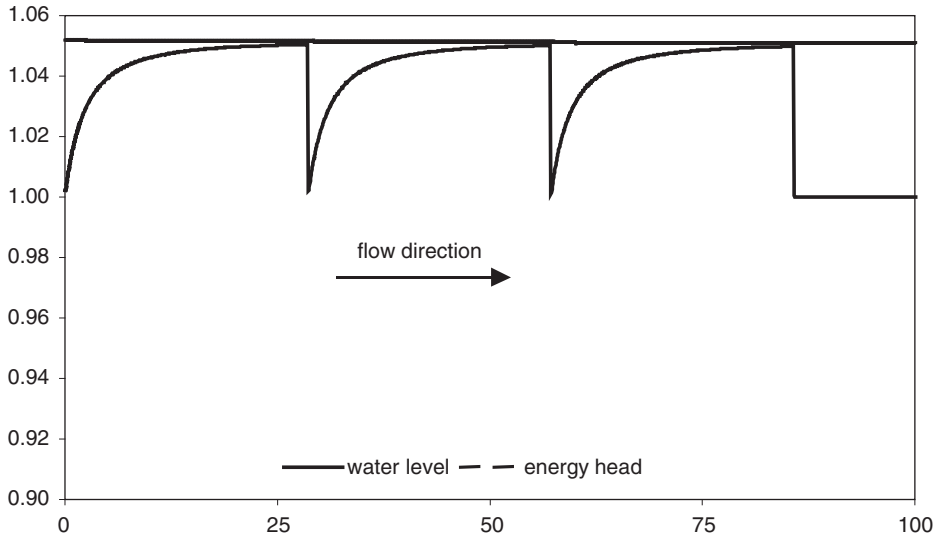

Figure 11. Water levels and energy line of method C.

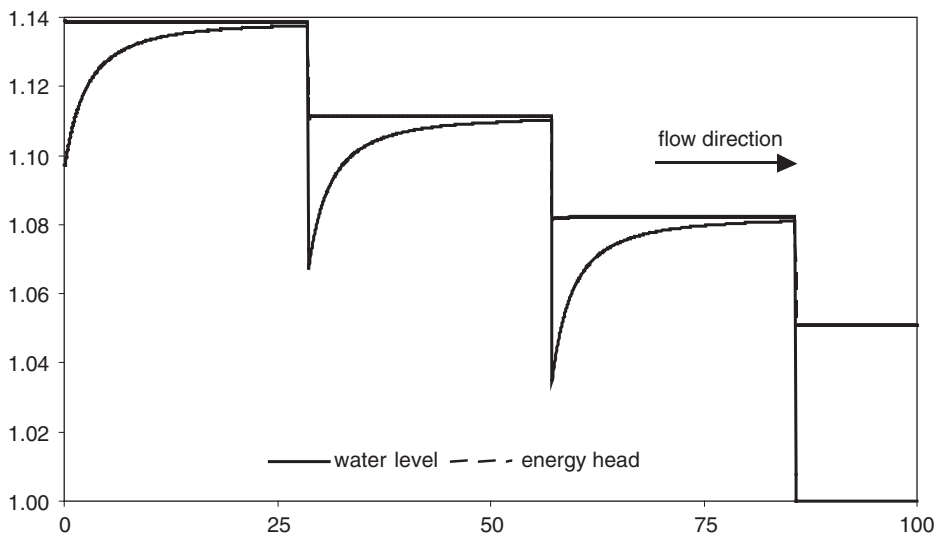

Figure 12. Water levels and energy line for Method D.

In summary the following conclusions are to be drawn:

1. Energy conserving methods will never generate head losses.
2. Momentum conserving methods generate head losses at sudden expansions but could generate an increased energy head at sudden contractions. The latter is wrong and dangerous for stability.

Copyright © 2003 John Wiley & Sons, Ltd.

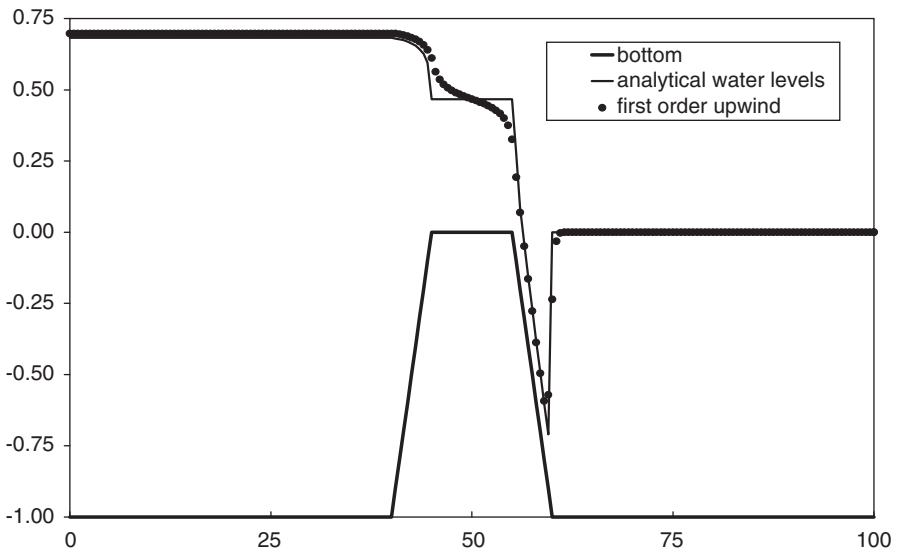

Figure 13. Hydraulic jump, first-order upwinding.

3. A combined approach, i.e. application of the momentum principle only in expansions and the Bernoulli equation in sudden contractions yields the best results in both cases.
4. The non-conservative approach will generate head losses at every sudden transition.

4.2. Hydraulic jump

This example is a steady state problem for a channel with a length of 100 m. In the middle of the channel of 10 m there is a sill with a crest of 1 m height, see Figure 3. At inflow a depth-integrated velocity is prescribed of 1 m^2/s and at outflow a water depth of 1 m. Down stream of the sill a hydraulic jump will develop. For the sill we consider two cases A and B. For case A the crest length is 10 m and the tangent of slopes at both sides is 0.2. For case B the crest length is 20 m and the slopes are abrupt, within 1 grid cell.

4.3. Hydraulic jump, case A

Figure 13 shows a comparison of the analytical and the first-order solution. It is to be noted that the depth-integrated velocity is precisely 1 m^2/s everywhere in the channel so mass conservation is exact. Figure 14 shows slightly improved accuracy, in particular on top of the crest and upstream from the sill, when the *Van Leer limiter* is applied. According to notions in open channel hydraulics, the average flow speed on the crest should be precisely critical as is indeed the case.

4.4. Hydraulic jump, case B

In the first example the slopes were smooth such that only in the hydraulic jump there is a rapid flow transition that necessitates proper local conservation properties. To illustrate the importance of proper conservation properties also near steep slopes, the slopes of the sill are

Copyright © 2003 John Wiley & Sons, Ltd.

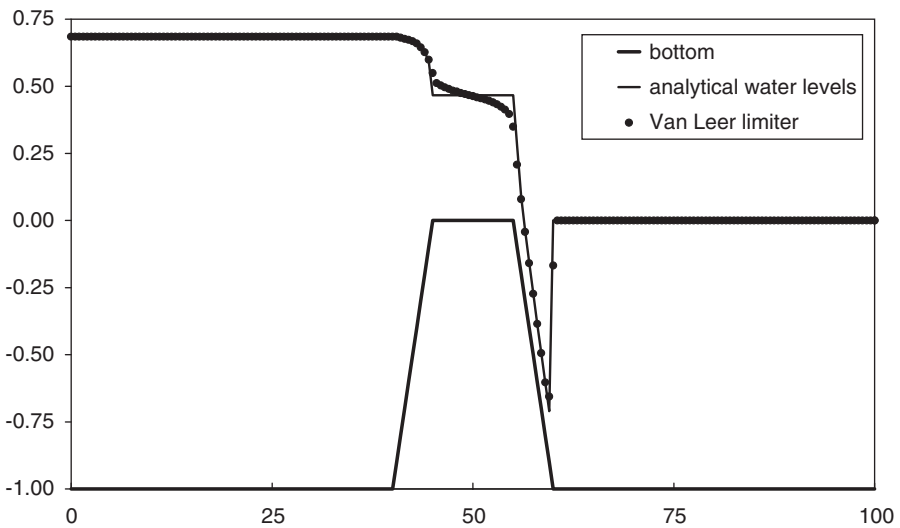

Figure 14. Hydraulic jump, extrapolation with Van Leer Limiter.

now abrupt within one grid cell. For the upstream part the water level should not be different from case A. To demonstrate the importance of a proper balance we consider three sub-cases:

1. Momentum balance everywhere, Method B
2. Energy head conservation everywhere, Method A
3. Energy head conservation in contractions and conservation of momentum elsewhere, Method D.

For all cases the *minmod* slope limiter has been applied, due to the better stability properties of this limiter in comparison to the Van Leer limiter.

Figure 15 shows the results for case B1. The upstream water level is 2.7 cm too low. The results for the water level are of reasonable accuracy however, when considering the energy line, errors become apparent. At the upstream slope the energy is increasing erroneously. On the crest the water level is correct and the flow is almost precisely critical. At the transition of the flat crest to the downstream slope the energy line shows an erroneous peak. Apparently the transition from critical to supercritical flow is incorrect in this case.

Figure 16 shows the results for case B2. The upstream water levels are exactly correct. However downstream of the sill the results are entirely erroneous. The jump is absent and the flow remains supercritical since energy dissipation cannot take place.

Figure 17 shows the results for case B3. Now the solution is correct everywhere. The energy line is constant everywhere, except near the hydraulic jump where the energy head drops as is to be expected by considerations based on open channel hydraulics.

4.5. Dam break

The second example is a classical dam break problem, as described by Stoker [26]. The length of the channel was 100 m and the grid size 1 cm. The time step has been chosen

Copyright © 2003 John Wiley & Sons, Ltd.

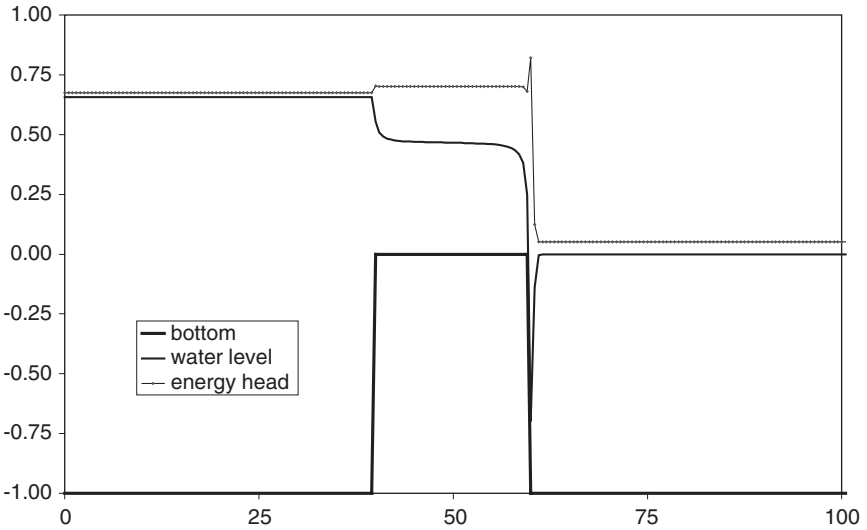

Figure 15. Steep bed slope with momentum balance at each grid point.

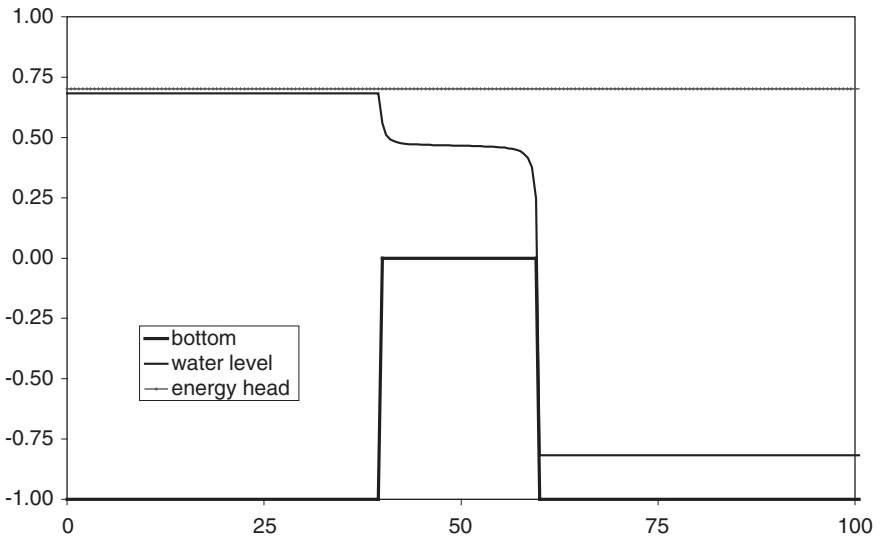

Figure 16. Steep bed slope with energy head balance at each grid point.

sufficiently small for convergence. Figures 18 and 19 show the dry bed test, which is also a good example to demonstrate the quality of flooding based upon non-negative water levels. Figure 18 also shows the importance of momentum conservation in the transition from dry to wet that involves a large discontinuity of the flow speed. With an energy head conserving approximation, at the transition from wet to dry, a bore will develop erroneously and the

Copyright © 2003 John Wiley & Sons, Ltd.

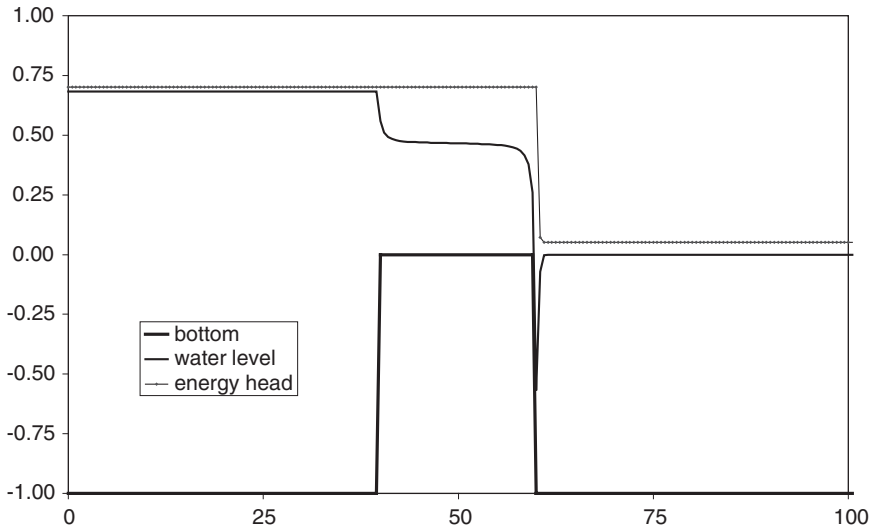

Figure 17. Steep bed slope with momentum balance or energy head balance, depending on local flow conditions.

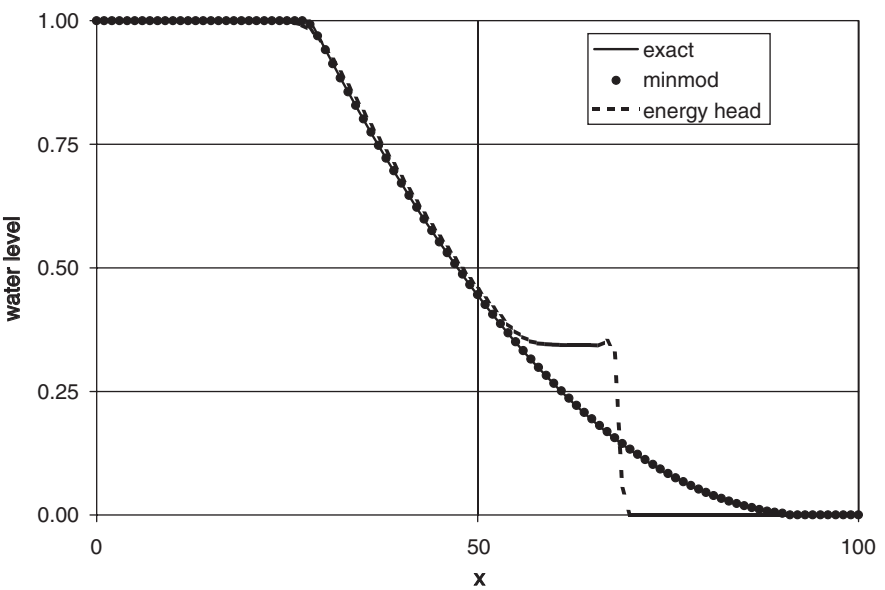

Figure 18. Dry bed dam break water levels.

flooding progresses to slowly. Figure 20 shows the flow speed. Figure 19 shows the wet bed case. The results are quite accurate. For all the dam break cases the minmod limiter has been applied.

Copyright © 2003 John Wiley & Sons, Ltd.

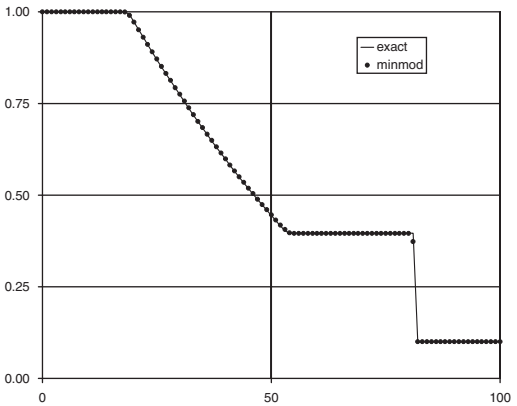

Figure 19. Wet bed dam break water levels.

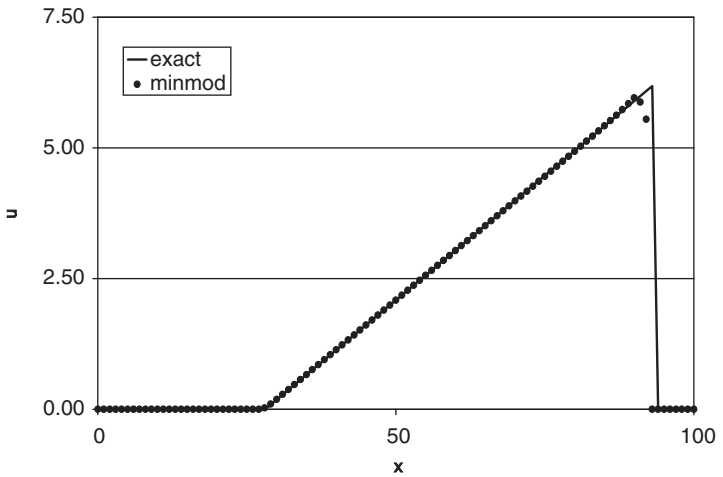

Figure 20. Dry bed dam break velocities.

5. TWO-DIMENSIONAL DAM BREAK AND FLOODING EXPERIMENTS

For testing the accuracy, a laboratory experiment has been executed. The experimental set-up consisted of two reservoirs, with different water levels; separated by a wall, see Figure 21. In the middle of the wall is a gate, which can be lifted. The gate had a constant width. When lifting the gate, one reservoir is flooded by water from the other one. For the numerical simulations, the grid size was 0.1 m resulting in approximately 25 000 grid points.

From the histogram of the water level in reservoir B, one can compute the mass flux through the aperture. The width of the gate was 0.40 m. The gate was lifted with a speed of 16 cm/ s. The initial water level in reservoir B was 0.6 m for every experiment. A couple of experiments were performed: (1) an experiment with an initial dry bed in reservoir A and (2) an experiment with an initial wet bed of 5 cm. Figure 22 shows a picture of the dry bed

Copyright © 2003 John Wiley & Sons, Ltd.

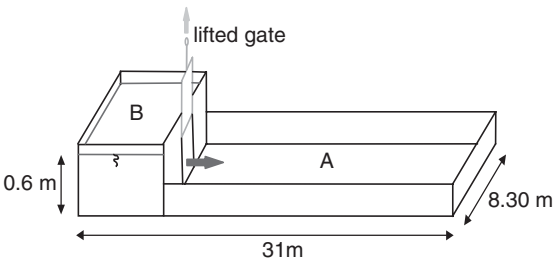

Figure 21. Basic set-up of the experiment.

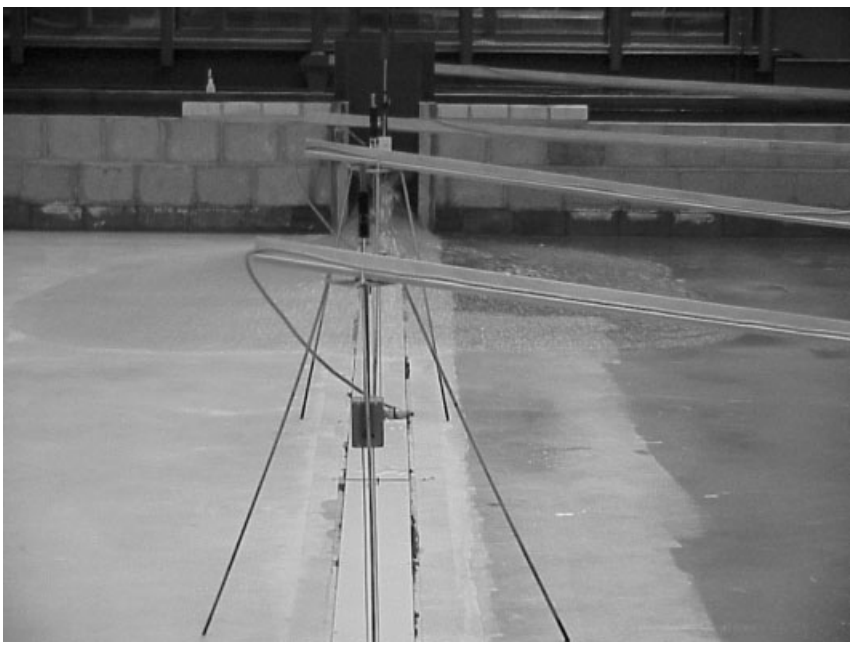

Figure 22. Dry bed laboratory experiment.

laboratory experiment. In the centre line of reservoirs water levels could be measured with wave gauges. The gauges were located along the centre line of B and at 1, 6, 9, 13, 17, 21 and 23 m from the opening. The propagation of the waterfront was recorded with cameras. Plate 1(a) shows the front on the dry bed as computed at $t = 4$ and 18 s. Figures 23 and 24 show the propagation of the front on the dry bed as measured and as computed at various time intervals and various values for the bed friction. The dry bed computations were sensitive to friction (Manning) values; see also Reference [27].

Plate 2 shows the water levels at the wave gauges, again as measured and as computed. The measurements compare reasonably well with the simulation results. In the gate the simulated water levels are too high, probably as a consequence of the lack of 3D contraction at the opening. It turned out to be very important to apply energy head conservation in the flow

Copyright © 2003 John Wiley & Sons, Ltd.

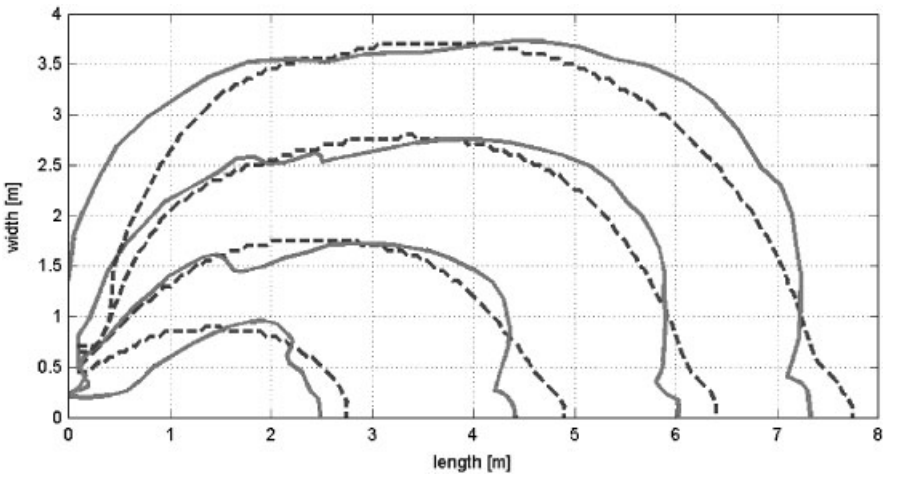

Figure 23. Dry bed experiment, front position at $t = 1, 2, 3, 4$ s, $n = 0012$ $\mathrm{m}^{-1/3}$ s. ▬▬ numerical results, $n = 0.012\,\mathrm{m}^{1/3}$ ▬ experimental results.

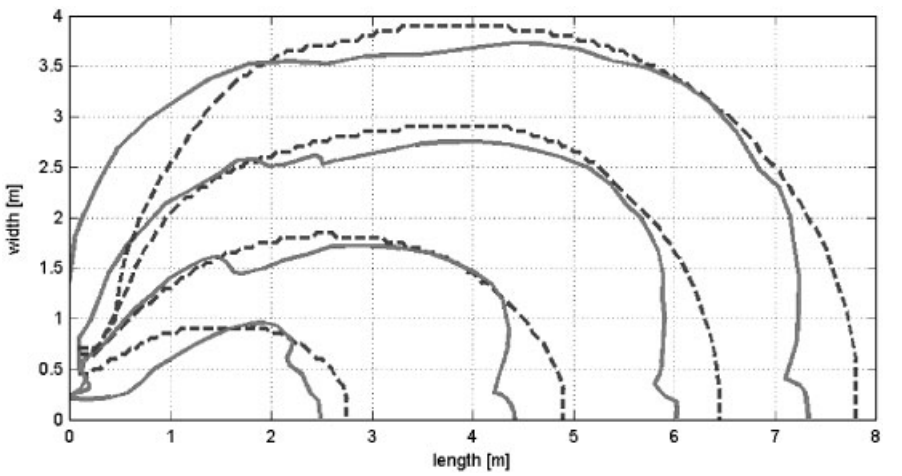

Figure 24. Dry bed experiment, front position at $t = 1, 2, 3, 4$ s, $n = 0.01\,\mathrm{m}^{-1/3}$ s: ▬▬ : numerical results, $n = 0.010\,\mathrm{m}^{-1/3}$ s and ▬ experimental results.

contraction of the gate otherwise very inaccurate results were obtained. In particular during the lifting of the gate, the flow under the gate changes from subcritical to supercritical. Everywhere else momentum conservation has been applied for this case. The results are sensitive to the friction values that were used; see the Figures 23 and 24.

The Plates 1(b) and 3, and Figure 25, in a similar way to the dry bed, present the wet bed results. They compare even better with the measurements. The influence of friction is small in the wet bed case so that the dynamical forces are dominant. Apparently this is represented quite accurately by the numerical approximations. Also the complex location of the hydraulic

Copyright © 2003 John Wiley & Sons, Ltd.

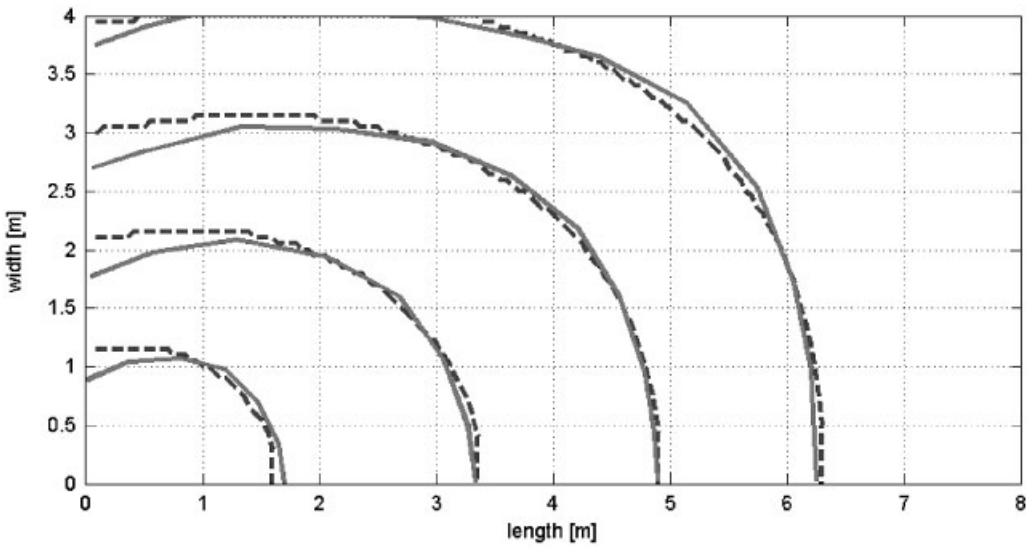

Figure 25. Wet bed experiment, bore front at $t = 1, 2, 3, 4$ s: ▬▬ : numerical results, $n = 0.012\ \mathrm{m}^{-1/3}$ s and ▬ experimental results.

jump and the reflections from the sidewalls, see Plate 1(b), are represented accurately as follows from the Figure 25 and Plate 3. As in the dry bed case it turned out to be very important to apply energy head conservation in the strongly contracting upstream part of the gate otherwise very inaccurate results were obtained. Everywhere else momentum conservation has been applied.

The method described in this paper is also applied for inundation disaster simulations in the Netherlands. Verification with historical data is given by Hesselink [28]. In Reference [29] a general overview of the role of models in flood management is given.

6. CONCLUDING REMARKS

Robust shallow water approximations, based upon primitive variables, can be constructed. They guarantee mass conservation, non-negative water levels and a correct momentum or energy head balance, depending on local flow conditions, near discontinuities. This yields efficient and accurate simulations of rapidly varied flows. The approach of non-negative water levels avoids the necessity of flooding procedures. Strict conservation of momentum is crucial for accurate estimation of energy losses in strong expansions of the flow, in particular if these expansions are shock phenomena. However, in strong flow contractions without shocks, it is better to apply advection approximations that are consistent with conservation of the head. This follows from physical principles of open channel hydraulics, and it will reduce bed slope source term problems significantly. Therefore, the momentum principle cannot be applied as a rigorous principle for robust solutions of shallow water equations. Although the scheme as presented here is not a truly 'Riemann solver', yet the results are accurate also for rapidly varied flows, while the method is implicit and based upon staggered grids. The efficiency of the semi implicit and staggered approach allows application to large-scale inundation problems.

Copyright © 2003 John Wiley & Sons, Ltd.

Finally, it is to be noted that most of the problems with rapidly varied flow are in essence due to the local invalidity of the hydrostatic pressure assumption in combination with depth averaged model formulations. The best way, from a physical point of view, to improve the accuracy is to apply 3D non-hydrostatic free surface model formulations.

REFERENCES

1. Leendertse JJ. *Aspects of a computer model for long period water-wave propagation*. RAND Corporation Memorandum RM-5294-PR,1967.
2. Casulli V. Semi-implicit finite differential methods for two-dimensional shallow water equation. *Journal of Computational Physics* 1990; **86**:56–74.
3. Vreugdenhil CB. *Numerical Methods for Shallow Water Flow*. Kluwer Academic Publishers: Dordrecht, 1994.
4. Stelling GS, van Kester JJ. On the approximation of horizontal gradients in sigma coordinates for bathymetry with steep bottom slopes. *International Journal for Numerical Methods in Fluids* 1995; **18**:915–935.
5. Casulli V, Catani E. Stability, accuracy and efficiency of a semi-implicit method for three-dimensional shallow water flow. *Computers & Mathematics with Application* 1994; **15**(6):629–648.
6. Wilders P, Th Van Steijn GS, Stelling, Fokkema GA. A fully implicit splitting method for accurate tidal computations. *International Journal for Numerical Methods in Engineering* 1988; **26**:2707–2721.
7. Casulli V, Zanolli P. Semi-implicit numerical modeling of nonhydrostatic free-surface problems for environmental problems. *Mathematical and Computer Modelling* 2002; **36**:1131–1149.
8. Wesseling P. *Principles of Computational Fluid Dynamics*. Springer: Berlin, 2000.
9. Casulli V, Stelling GS. Numerical simulation of 3D quasi-hydrostatic free-surface flows. *Journal of Hydraulic Engineering* 1998; **124**(7):678–686.
10. Casulli V. A semi-implicit finite difference method for nonhydrostatic, free-surface flows. *International Journal for Numerical Methods in Fluids* 1999; **30**:425–440.
11. Stelling GS, Busnelli MM. Numerical simulation of the vertical structure of discontinuous flows. *International Journal for Numerical Methods in Fluids* 2001; **37**:23–43.
12. Arakawa A. Computational design for long-term numerical integration of the equations of fluid motion: two-dimensional incompressible flow. Part I. *Journal of Computational Physics* 1966; **1**(1):119–143.
13. Zhou JG, Stansby PK. 2D shallow water model for the hydraulic jump. *International Journal for Numerical Methods in Fluids* 1999; **29**:375–387.
14. Toro EF. *Riemann Solvers and Numerical Methods for Fluid Dynamics*. Springer: Berlin, 1999.
15. Glaister P. Approximate Riemann solutions of the shallow water equations. *Journal of Hydraulic Research* 1988; **26**:293–206.
16. Alcrudo F, Garcia-Navarro P. A high-resolution Godunov-type scheme in finite volumes for the 2-d shallow water equations. *International Journal for Numerical Methods in Fluids* 1993; **16**:489–505.
17. Brufau P, Vazquez-Cendon ME, Garcia-Navarro P. A numerical method for the flooding and drying of irregular domains. *International Journal for Numerical Methods in Fluids* 2002; **39**:247–275.
18. Chow VT. *Open-Channel Hydraulics*. McGraw-Hill Book Company: New York, 1959.
19. Chanson H. *The Hydraulics of Open Channel Flow*. Arnold publishers/Wiley: Paris/New York, 1999.
20. Bijl H, Wesseling P. A unified method for incompressible and compressible flows in boundary-fitted coordinates. *Journal of Computational Physics* 1998; **141**:153–173.
21. Stelling GS, Wiersma A, Willemse JBThM. Practical aspects of accurate tidal computations. *Journal ASCE Hydraulic Engineering* 1986; **9**:802.
22. Falconer RA, Chen Y. An improved representation of flooding and drying and wind stress effects in a 2D tidal numerical model. *Proceedings of the Institution of Civil Engineers Part 2* 1991; **2**:659–672.
23. Hirsch C. *Numerical Computation of Internal and External Flows*. Wiley: New York, 1990.
24. Stelling GS. On the construction of computational methods for shallow water flow problems. *Rijkswaterstaat communication* 1984; **35**:129–168.
25. Goutal N, Maurel F. A finite volume solver for 1D shallow-water equations applied to an actual river. *International Journal for Numerical Methods in Fluids* 2002; **38**:1–19.
26. Stoker JJ. Water waves. *Pure and Applied Mathematics*, vol. IV. Interscience Publishers: New York, 1957.
27. Dressler RF. Comparison of theories and experiments for the hydraulic dam-break wave. *National Bureau of Standards*, Washington, D.C., U.S.A., 1975.
28. Hesselink AW. History makes a river. Morphological changes and human interference in the river Rhine, The Netherlands. *Netherlands Geographical studies* 2002; **292**:124–144.
29. Battjes JA, Gerritsen HA. Coastal modelling for flood defense. *Philosophical Transaction of The Royal Society* 2002; **360**(1796):1461–1475.

Copyright © 2003 John Wiley & Sons, Ltd.

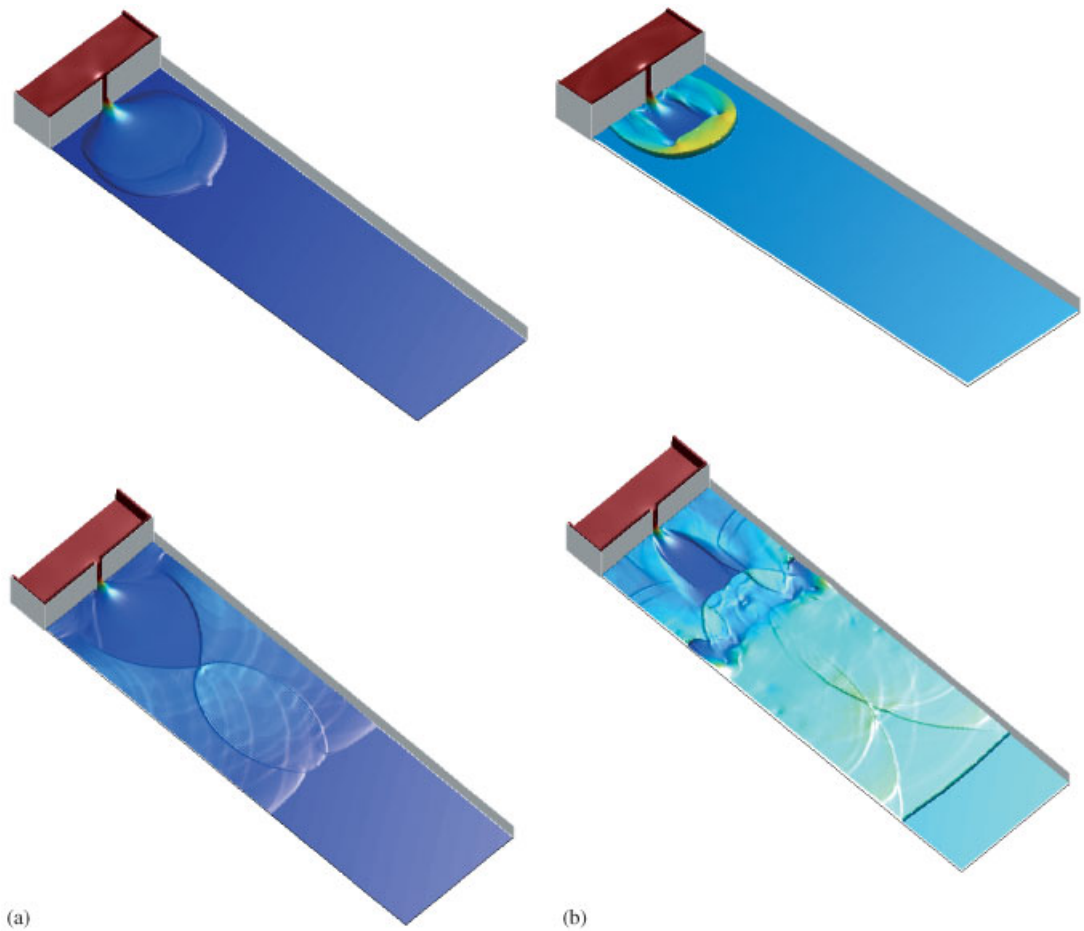

Plate 1. (a) Dry bed experiment, water levels at $t = 4$ and 18 s. (b) Wet bed experiment, water levels at $t = 3$ and 18 s.

Copyright © 2003 John Wiley & Sons, Ltd.

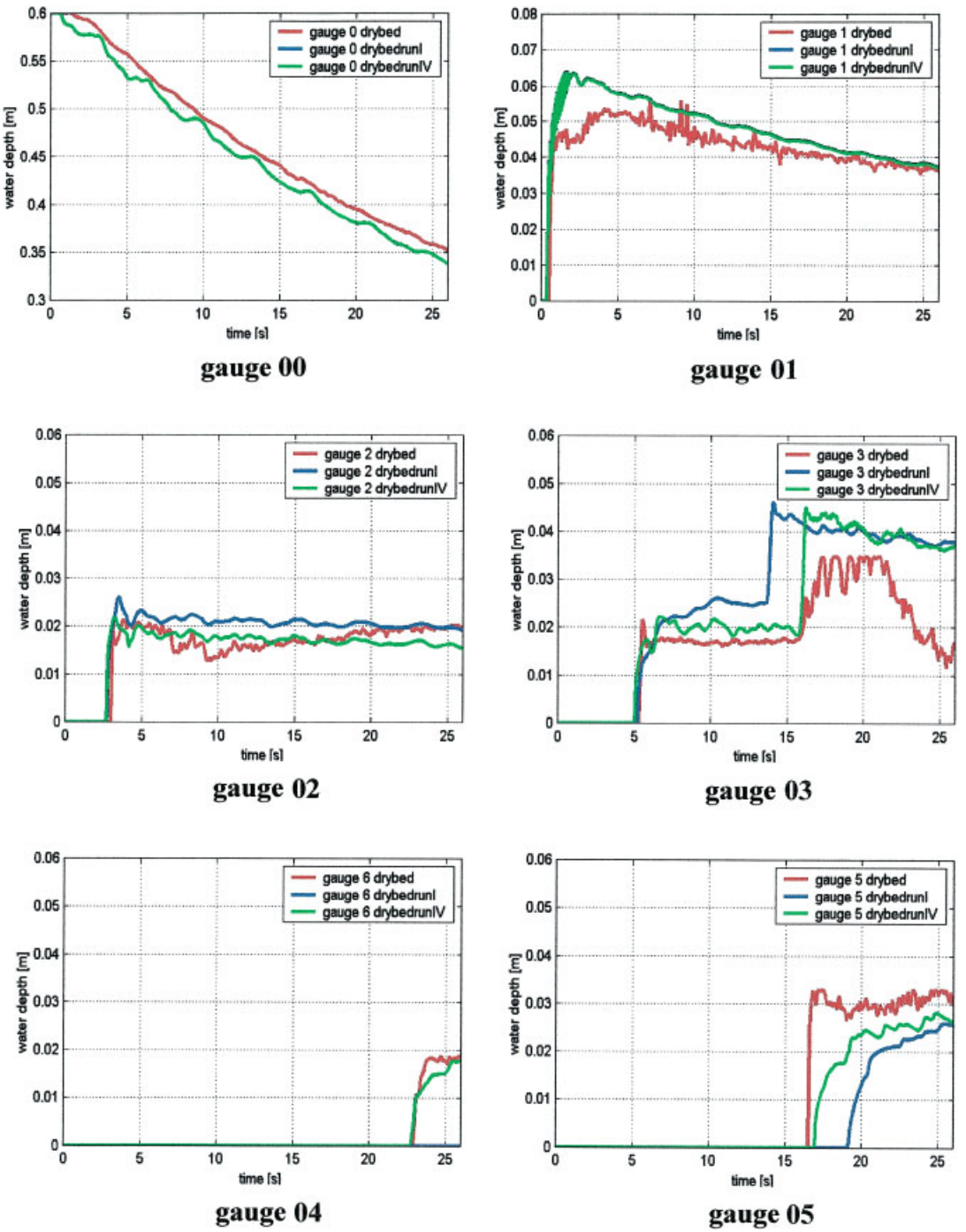

Plate 2. Water levels at gauges as measured and as computed for $n = 0.012$ and 0.01.

Copyright © 2003 John Wiley & Sons, Ltd.

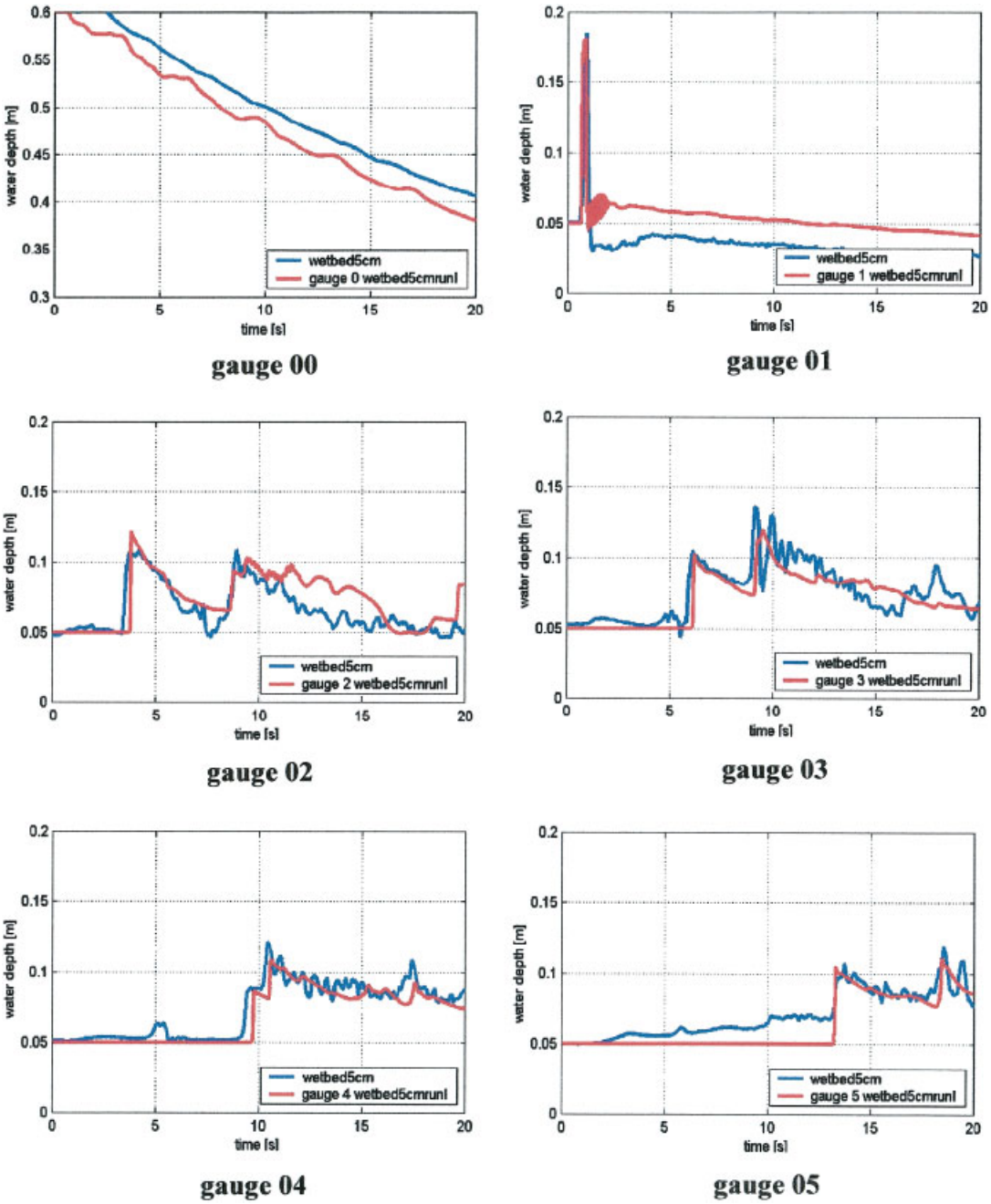

Plate 3. Wet bed experiment, water levels as measured and as computed.

Copyright © 2003 John Wiley & Sons, Ltd.